Am J Cancer Res 2024;14(10):4909-4921
www.ajcr.us /ISSN:2156-6976/ajcr0159258

Original Article

Identification of high-risk tumor characteristics in patients with localized prostate cancer using conventional combined with diffusion-weighted MRI imaging parameters

Min Wang, Jianrong Wen, Peijun Liu

Department of Radiology, The Affiliated Nanhua Hospital, Hengyang Medical School, University of South China, Hengyang 421002, Hunan, China

Received July 17, 2024; Accepted October 12, 2024; Epub October 15, 2024; Published October 30, 2024

Abstract: The objective of this study was to investigate the utility of conventional imaging combined with diffusion-weighted magnetic resonance imaging (MRI) in identifying high-risk tumor characteristics in patients with localized prostate cancer. A retrospective cohort study was conducted on 194 patients who underwent surgery for localized prostate cancer. Patients were categorized into low-risk and high-risk groups based on clinical criteria. Imaging data were obtained using a MRI system, and various imaging parameters were analyzed, including T1-weighted imaging (T1WI), T2-weighted imaging (T2WI) signal intensities, diffusion-weighted MRI parameters, and their correlations with clinical characteristics. Statistical methods such as logistic regression, and receiver operating characteristic (ROC) analysis were employed to assess the diagnostic performance of the imaging parameters and to construct joint prediction models. A verification set prediction model was established and compared. The comparison of demographic and clinical characteristics between the low and high-risk groups revealed significant differences in the prostate-specific antigen (PSA) level, Gleason score, Tumor Size and prostate volume (PV). Standard imaging parameters, T1WI and T2WI signal intensities, exhibited significant differences between the low and high-risk groups. Additionally, diffusion-weighted MRI parameters, including signal intensities at different b values, apparent diffusion coefficient (ADC), K^{trans}, and K_{ep}, were notably associated with high-risk tumor characteristics in localized prostate cancer. Logistic regression analysis identified both standard imaging and diffusion-weighted MRI parameters as independent predictors of high-risk tumor characteristics. Furthermore, the ROC analysis demonstrated the diagnostic potential of T2WI signal intensity, signal intensity at 800 s/mm^2, and ADC in identifying high-risk tumors. Joint prediction models combining standard imaging and diffusion-weighted MRI parameters showed high predictive accuracy for high-risk tumor characteristics in localized prostate cancer, with Area Under the Curve (AUC) values of 0.777 for standard imaging, 0.826 for diffusion-weighted MRI, and 0.892 for the combined model. The AUC value for the prediction model in validation set was 0.860. In conclusion, this study underscores the diagnostic potential of conventional imaging combined with diffusion-weighted MRI in identifying high-risk tumor characteristics in patients with localized prostate cancer. Both standard imaging and diffusion-weighted MRI parameters were identified as non-invasive biomarkers for risk assessment and prognosis. These findings have implications for precision treatment of localized prostate cancer, highlighting the potential integration of imaging-based risk assessment tools into clinical practice for tailored treatment strategies and improved patient outcomes.

Keywords: High-risk tumor characteristics, localized prostate cancer, conventional imaging, diffusion-weighted MRI enhancement

Introduction

Prostate cancer is one of the most prevalent malignancies affecting men worldwide, representing a significant public health concern [1, 2]. According to global cancer statistics, prostate cancer ranks as the second most diagnosed cancer and the fifth leading cause of cancer-related mortality in men [3, 4]. The characteristics of prostate cancer encompasses a diverse spectrum of disease presentations, ranging from indolent, localized tumors to

https://doi.org/10.62347/XADT5737

aggressive, metastatic disease [5, 6]. Effective risk stratification is paramount in guiding treatment decisions and optimizing outcomes in patient with localized prostate cancer.

Traditionally, risk stratification in prostate cancer has relied on clinical parameters such as prostate-specific antigen (PSA) levels [7-9], Gleason score [10-12], and tumor stage [13], which are derived from histopathological assessment. These parameters serve as cornerstones in risk assessment and appropriate management approach determination, including active surveillance, surgery, radiation therapy, or systemic therapy. However, the inherent limitations of traditional risk stratification tools underscore the need for adjunctive methods that can augment risk assessment accuracy and refine treatment decision-making.

Imaging modalities play a pivotal role in the diagnostic and prognostic evaluation of prostate cancer, offering insights into the anatomical and functional characteristics of tumors. Conventional imaging techniques, including magnetic resonance imaging (MRI), provide valuable information on the location, extent, and morphology of prostate tumors, aiding in treatment planning and disease staging [14]. Moreover, advanced MRI sequences, such as diffusion-weighted imaging (DWI), have shown promise in delineating tumor microstructure and assessing vascular perfusion, respectively [15].

This study aimed to investigate the utility of conventional imaging combined with diffusion-weighted MRI in identifying high-risk tumor characteristics in patients with localized prostate cancer. By integrating the macroscopic insights from conventional imaging with the microstructural assessments provided by diffusion-weighted MRI, this study sought to evaluate the potential of this comprehensive imaging approach in risk stratification and prognostication in localized prostate cancer.

Materials and methods

Study design

This study was approved by the Ethics Committee and Institutional Review Board of the Affiliated Nanhua Hospital, Hengyang Medical School, University of South China. Informed consent for this retrospective study was waived as only de-identified patient data was used, with no potential harm or impact on patient care.

Clinical data were collected from patients with localized prostate cancer who underwent surgery at the Affiliated Nanhua Hospital of Hengyang Medical School from January 2023 to June 2023. Patients were categorized into low-risk (n = 101) and high-risk (n = 93) groups based on Gleason Scores (GS) ≥ 8 or PSA levels ≥ 20 ng/mL.

Inclusion and exclusion criteria

Inclusion criteria: Patients meeting diagnostic criteria for localized prostate cancer [16]; TNM stage T2; Patients who underwent radical prostatectomy within one month; Patients confirmed to have prostate cancer confined to the capsule after radical prostatectomy; Age > 18 years; Normal mental and cognitive function; Complete medical records.

Exclusion criteria: Simultaneous involvement of the peripheral zone and central gland of the prostate; Patients who underwent transrectal biopsy and treatment before the MRI examination; Concurrent other cancers; Patients with significant organ diseases (e.g., heart, liver, kidney); Benign prostatic hyperplasia; Presence of bone metastases or distant metastases; Patients with poor general condition unable to undergo surgical treatment.

Examination method

MRI examination: The MRI examinations were performed using an MRI system (SIGNA Pioneer 3.0T, GE, USA) with a 32-channel body coil. Patients were instructed to drink a small amount of water before the MRI examination to moderately fill the bladder. For the examination, the body coil was placed at the pubic symphysis, and the scanning range included the prostate and seminal vesicles. (1) MRI Plain Scan: Transverse T1-weighted imaging (T1WI) sequences (TR 500 ms, TE 13 ms), transverse T2-weighted imaging (T2WI) sequences (TR 6000 ms, TE 110 ms), transverse fat-suppressed T2WI sequences (TR 1483 ms, TE70 ms), and coronal fat-suppressed T2WI sequences (TR 5189 ms, TE 98 ms) were used to scan and assess the overall condition of the pros-

tate and seminal vesicles, and to observe for any metastases [17]. DWI Examination: A single-shot spin-echo echo-planar imaging sequence was selected with transverse scan orientation and the following parameters: TR 3200 ms, TE 90 ms, slice gap 0.5 mm, slice thickness 4.0 mm, field of view 300 mm × 300 mm, matrix 256 × 256, with diffusion sensitivities (b-values) of 50 s/mm^2 and 800 s/mm^2. A no-gap scan was performed for 100 s, and the apparent diffusion coefficient (ADC) map was automatically generated by the MRI console.

MRI image processing: The MRI images obtained from the scans were saved to the GE SIGNATM post-processing workstation for image analysis, measuring the signal intensities of T1WI and T2WI images. In the analysis of the ADC map derived from diffusion-weighted imaging, the center of the lesion was selected as the region of interest (ROI), and the signal intensities at different b-values, as well as the ADC value of the lesion, were measured, with three consecutive measurements taken and averaged. In the analysis of imaging, the most prominently enhanced region within the lesion was selected as the ROI, and a time-intensity curve (TIC) was plotted, with measurements of the transfer constant (K^{trans}) and rate constant (K_{ep}) for the ROI were recorded.

Detection indicators

In this study, a systematic retrieval of patient information was performed, including age, body mass index (BMI), smoking history, alcohol intake history, hypertension, diabetes, hyperlipidemia, family history of prostate cancer, PSA level, and Gleason score. Prior to the surgery, 5 mL of fasting venous blood was drawn from each patient, centrifuged at 3,000 rpm for 10 minutes to obtain serum, and the serum PSA level was determined using chemiluminescence immunoassay. Pathological examination was conducted on all excised tumor tissues, and the Gleason score was determined according to the Prostate Cancer Pathological Grading Consensus [18]. Serological parameters included white blood cell (WBC) count, red blood cell (RBC) count, hemoglobin (Hb) levels, mean platelet volume (MPV), neutrophil-to-lymphocyte ratio (NLR), lymphocyte-to-monocyte ratio (LMR), platelet-to-lymphocyte ratio (PLR), neutrophil count, lymphocyte count, monocyte count, and platelet count. 4 mL of fasting venous blood from was drawn from all patients in the morning, left to stand for 2 hours, centrifuged at 3,000 rpm for 10 minutes, and the upper serum was stored in a refrigerator at -20°C for later use. The NLR, LMR, and PLR values were measured using an automated blood cell analyzer (Sysmex Corporation, XT-4000i).

Statistical methods

Data analysis was conducted using SPSS 29.0 statistical software (SPSS Inc., Chicago, IL, USA). Categorical data were presented as [n (%)] and chi-square tests were performed using the basic formula when the sample size was ≥ 40 and the theoretical frequency T was ≥ 5. For sample sizes ≥ 40 but theoretical frequencies $1 \leq T < 5$, a corrected formula chi-square test was utilized. When the sample size was < 40 or the theoretical frequency T < 1, statistical analysis was performed using Fisher's exact probability test. The Shapiro-Wilk method was used to assess the normality of continuous variables. Normally distributed continuous variables were expressed as ($\bar{x} \pm s$), and a corrected variance t-test was employed. Non-normally distributed data were presented in the form of median (25th percentile, 75th percentile) and analyzed using the Wilcoxon rank-sum test. A two-sided *P* Value of < 0.05 was considered statistically significant. Pearson correlation analysis was performed for continuous variables. Variables showing significant differences in both the difference and correlation analyses were included as covariates for logistic regression analysis. The area under the receiver operating characteristic (ROC) curve (AUC) was used to evaluate the diagnostic performance of diffusion-weighted MRI alone, standard imaging, and combined approach for the high-risk tumor features of localized prostate cancer. A joint prediction model was constructed using the Gradient Boosting Machine (GBM) algorithm. The GBM algorithm initially calculates pseudo-residuals based on the initial model, then builds a base learner to interpret the pseudo-residuals, which decreases the residuals in the gradient direction. The base learner was then multiplied by a weighting coefficient (learning rate) and combined with the original model to form a new model. This was iterated to find a model that minimizes the expected loss function. Additionally, the nnet and pls algorithms

Table 1. Comparison of general information and demographic characteristics between the low- and high-risk groups

Characteristic	Low Risk Group (n = 101)	High Risk Group (n = 93)	t/χ^2	*P* Value
Age (years)	60.75 ± 5.32	62.21 ± 6.44	1.714	0.088
BMI (kg/m^2)	26.65 ± 1.89	27.08 ± 2.21	1.443	0.151
Smoking history	28 (27.72%)	23 (24.73%)	0.096	0.757
Alcohol consumption history	15 (14.85%)	15 (16.13%)	0.002	0.962
Hypertension [n (%)]	49 (48.51%)	42 (45.16%)	0.105	0.746
Diabetes [n (%)]	30 (29.7%)	24 (25.81%)	0.198	0.657
Hyperlipidemia [n (%)]	43 (42.57%)	36 (38.71%)	0.161	0.688
Family history of prostate cancer (Yes/No)	30 (29.7%)	37 (39.78%)	1.754	0.185
PSA level (ng/mL)	18.34 ± 6.21	21.78 ± 1.52	5.392	*P* < 0.001
Gleason score	7.53 ± 1.52	8.23 ± 1.61	3.087	0.002

Notes: BMI: body mass index; PSA: prostate-specific antigen.

Table 2. Comparison of tumor characteristics between the low- and high-risk groups

Characteristic	Low Risk Group (n = 101)	High Risk Group (n = 93)	t/χ^2	*P* Value
Tumor Size (cm)	3.45 ± 1.55	4.76 ± 2.25	4.689	*P* < 0.001
PV/mL	42.16 ± 8.32	38.43 ± 8.92	3.008	0.003
Tumor location			None	0.067
Peripheral zone	51 (50.5%)	52 (55.91%)		
Central zone	21 (20.79%)	15 (16.13%)		
Transition zone	26 (25.74%)	18 (19.35%)		
Periurethral	3 (2.97%)	2 (2.15%)		
Lymph	0 (0.00%)	6 (6.45%)		
Pathological Stage			7.475	0.024
T1	31 (30.69%)	25 (26.88%)		
T2	46 (45.54%)	58 (62.37%)		
T3	24 (23.76%)	10 (10.75%)		

Note: PV: prostate volume.

were also employed to construct the joint prediction model.

To validate the model, an additional 150 patients from July 2023 to December 2023 who met the requirements were included as the validation set. These patients were divided into high-risk and low-risk groups using the same method as the primary analysis. The data in the model were collected and ROC analysis was carried out to establish the validation set prediction model.

Results

General information

In this study, the general demographic characteristics of patients in low (n = 101) and high (n = 93) risk groups were compared. No significant differences were observed in age, BMI, smoking history, alcohol consumption, hypertension, diabetes, hyperlipidemia, or family history of prostate cancer (all $P > 0.05$) between the high and low risk groups. However, PSA levels ($t = 5.392$, $P < 0.001$) and Gleason scores ($t = 3.087$, $P = 0.002$) were significantly higher in the high-risk group compared to the low-risk group (**Table 1**). These findings underscore the importance of PSA levels and Gleason scores in distinguishing between low- and high-risk prostate cancer patients.

Tumor characteristics

As shown in **Table 2**, significant differences were found in tumor size ($P < 0.001$), prostate volume (PV)/mL ($P = 0.003$), and pathological stage ($P = 0.024$) between the low and high risk groups. High-risk group demonstrated larger tumors, lower prostate volume, and more advanced stages, especially T2 and T3, compared to the low-risk group. Tumor location did not differ significantly between the two groups ($P > 0.05$).

Blood routine findings

In terms of hematological parameters, no significant differences were observed between the low risk and high risk groups in terms of

Table 3. Comparison of blood routine indices between the low- and high-risk groups

Characteristic	Low Risk Group (n = 101)	High Risk Group (n = 93)	t/χ^2	*P* Value
Hemoglobin (g/L)	134.21 ± 10.41	135.27 ± 9.35	0.747	0.456
Red blood cell count (× 10^{12}/L)	4.35 ± 0.52	4.41 ± 0.47	0.729	0.467
White blood cell count (× 10^9/L)	6.05 ± 1.08	6.14 ± 1.14	0.573	0.567
Neutrophil count (× 10^9/L)	4.27 ± 0.82	4.33 ± 0.75	0.605	0.546
Platelet count (× 10^9/L)	218.71 ± 14.72	220.68 ± 13.09	0.991	0.323

Table 4. Comparison of MRI plain scan parameters between the low- and high-risk groups

Parameter	Low risk (n = 101)	High risk (n = 93)	t	*P* Value
T1WI signal intensity	289.24 ± 30.18	259.15 ± 40.16	5.862	*P* < 0.001
T2WI signal intensity	303.25 ± 20.15	283.36 ± 30.28	5.339	*P* < 0.001

Table 5. Comparison of diffusion-weighted MRI parameters between the low- and high-risk groups

MRI Characteristic		Low Risk Group (n = 101)	High Risk Group (n = 93)	t	*P* Value
Signal Intensity	50 s/mm^2	86.77 ± 7.75	95.68 ± 8.02	7.850	*P* < 0.001
	800 s/mm^2	101.56 ± 11.42	113.68 ± 9.64	8.006	*P* < 0.001
ADC (10^{-5} mm^2/s)		107.84 ± 12.64	95.64 ± 13.58	6.461	*P* < 0.001
Transfer constant (K^{trans})		0.29 ± 0.07	0.37 ± 0.09	6.797	*P* < 0.001
Rate constant (K_{ep})		0.67 ± 0.08	0.74 ± 0.06	6.611	*P* < 0.001

Note: ADC: apparent diffusion coefficient.

hemoglobin level, RBC count, WBC count, neutrophil count, or platelet count (all $P > 0.05$, **Table 3**). These findings suggest that hematological characteristics are comparable across risk groups.

MRI plain scan findings

In this study, the comparison of plain scan MRI parameters between the low-risk and high-risk groups yielded significant differences in T1WI and T2WI signal intensities. The T1WI signal intensity was notably lower in the high-risk group compared to the low-risk group (259.15 ± 40.16 vs. 289.24 ± 30.18, $t = 5.862$, $P < 0.001$). Similarly, the T2WI signal intensity was significantly lower in the high-risk group when compared to the low-risk group (283.36 ± 30.28 vs. 303.25 ± 20.15, $t = 5.339$, $P < 0.001$) (**Table 4**). These findings indicate that conventional MRI plain scans hold promise in identifying high-risk tumor characteristics in patients with localized prostate cancer.

Diffusion-weighted MRI findings

As shown in **Table 5**, a comparison of diffusion-weighted MRI (DWI) characteristics between the two groups revealed significant differences. In the high-risk group, the signal intensities at b values of 50 s/mm^2 and 800 s/mm^2 were notably higher, with mean values of 95.68 ± 8.02 and 113.68 ± 9.93, respectively, compared to 86.77 ± 7.75 and 101.56 ± 11.42 in the low-risk group (all $P < 0.001$). Furthermore, the ADC at 10^{-5} mm^2/s was significantly lower in the high-risk group (95.93 ± 13.58) compared to the low-risk group (107.84 ± 12.93) ($P < 0.001$). Additionally, the diffusion parameters, K^{trans} and K_{ep}, were markedly higher in the high-risk group, with mean values of 0.37 ± 0.09 and 0.74 ± 0.06, respectively, compared to 0.29 ± 0.07 and 0.67 ± 0.08 in the low-risk group (all $P < 0.001$). These findings suggest a potential association between diffusion-weighted MRI and high-risk tumor characteristics in localized prostate cancer.

Correlation analysis

The correlation analysis of standard and diffusion-weighted MRI parameters with high-risk features of localized prostate cancer (**Table 6**) revealed several significant associations. PSA level exhibited a positive correlation with high-risk features ($r = 0.351$, $P < 0.001$), as did the

Table 6. Correlation analysis of standard/diffusion-weighted MRI parameters with high-risk features of localized prostate cancer

	R	*P* Value
PSA level (ng/mL)	0.351	*P* < 0.001
Gleason score	0.218	0.002
Tumor Size (cm)	0.325	*P* < 0.001
PV/mL	-0.213	0.003
T1WI signal intensity	-0.393	*P* < 0.001
T2WI signal intensity	-0.365	*P* < 0.001
Signal Intensity (50 s/mm^2)	0.493	*P* < 0.001
Signal Intensity (800 s/mm^2)	0.498	*P* < 0.001
ADC (10^{-5} mm^2/s)	-0.424	*P* < 0.001
Transfer constant (K^{trans})	0.445	*P* < 0.001
Rate constant (K_{ep})	0.426	*P* < 0.001
Pathological Stage	-0.068	0.343

Notes: PSA: prostate-specific antigen; PV: prostate volume; ADC: apparent diffusion coefficient.

Gleason score (r = 0.218, P = 0.002) and tumor size (r = 0.325, P < 0.001). Conversely, T1WI and T2WI signal intensities demonstrated negative correlations with high-risk features (r = -0.393, P < 0.001 and r = -0.365, P < 0.001, respectively). Furthermore, signal intensities at b values of 50 s/mm^2 and 800 s/mm^2, K^{trans}, and K_{ep} all displayed significant positive correlations with high-risk features (r = 0.493, P < 0.001; r = 0.498, P < 0.001; r = 0.445, P < 0.001; r = 0.426, P < 0.001; respectively). Notably, the ADC, showed a significant negative correlation with high-risk features (r = -0.424, P < 0.001). The correlation between high-risk features and pathological stage was not significant (r = -0.068, P = 0.343). These findings indicate that both standard imaging parameters and diffusion-weighted MRI parameters were correlated with high-risk features of localized prostate cancer.

Logistic regression analysis

The risk prediction analysis for high-risk features in localized prostate cancer utilizing standard imaging and diffusion-weighted MRI parameters (**Table 7**) demonstrated notable findings. Tumor size (coef = 0.362, O*R* = 1.436), PSA level (coef = 0.181, O*R* = 1.198), signal intensity at 50 s/mm^2 (coef = 0.143, O*R* = 1.154), signal intensity at 800 s/mm^2 (coef = 0.112, O*R* = 1.119), transfer constant (K^{trans}) (coef = 12.972, O*R* = 430058.626), and rate constant (K_{ep}) (coef = 13.607, O*R* = 811673.44) were positively associated with high-risk status. Conversely, PV/mL (coef = -0.051, O*R* = 0.95) and ADC (coef = -0.071, O*R* = 0.931) were negatively associated with high-risk status. Additionally, T1WI and T2WI signal intensities also showed negative associations (coef = -0.025, O*R* = 0.976 for T1WI; coef = -0.031, O*R* = 0.97 for T2WI). Gleason score (coef = 0.286, O*R* = 1.331) was another significant predictor. These findings indicate that both standard imaging parameters and diffusion-weighted MRI parameters are independent risk factors for high-risk features of localized prostate cancer.

ROC analysis

The predictive value of standard imaging and diffusion-weighted MRI parameters for high-risk status in localized prostate cancer was assessed, as shown in **Table 8**. AUC for various diagnostic parameters in distinguishing between low- and high-risk prostate cancer cases yielded the following results: PSA level (AUC = 0.696), Gleason score (AUC = 0.619), tumor size (AUC = 0.677), PV/mL (AUC = 0.620), T1WI signal intensity (AUC = 0.718), T2WI signal intensity (AUC = 0.707), signal intensity at 50 s/mm^2 (AUC = 0.801), signal intensity at 800 s/mm^2 (AUC = 0.783), ADC (AUC = 0.749), transfer constant (K^{trans}) (AUC = 0.765), and rate constant (K_{ep}) (AUC = 0.745). These findings highlight the potential of these parameters in predicting high-risk status in localized prostate cancer.

Predictive value of joint model integrating standard MRI parameters for high-risk features in localized prostate cancer

As shown in **Figure 1**, the standard MRI parameters were combined to construct a joint model for predicting high-risk tumor characteristics in localized prostate cancer. The results revealed an AUC value of 0.777, higher than individual biomarkers. This suggests that the combined model of standard MRI imaging parameters holds predictive value for high-risk tumor characteristics in localized prostate cancer.

Predictive value of joint model integrating diffusion-weighted MRI parameters for high-risk features in localized prostate cancer

As depicted in **Figure 2**, the diffusion-weighted MRI enhancement parameters were combined

Table 7. Logistic regression analysis of various MRI parameters for high-risk characteristics in localized prostate cancer

Parameter	coef	Odds ratio	B	beta	*P* Value
Tumor Size (cm)	0.362	1.436	4.295	0.362	*P* < 0.001
PV/mL	0.051	0.95	2.898	-0.051	0.004
PSA level (ng/mL)	0.181	1.198	4.437	0.181	*P* < 0.001
Gleason score	0.286	1.331	2.969	0.286	0.003
T1WI signal intensity	0.025	0.976	5.053	-0.025	*P* < 0.001
T2WI signal intensity	0.031	0.97	4.75	-0.031	*P* < 0.001
Signal Intensity (50 s/mm^2)	0.143	1.154	6.103	0.143	*P* < 0.001
Signal Intensity (800 s/mm^2)	0.112	1.119	6.059	0.112	*P* < 0.001
ADC (10^{-5} mm^2/s)	0.071	0.931	5.396	-0.071	*P* < 0.001
Transfer constant (K^{trans})	12.972	430058.626	5.600	12.972	*P* < 0.001
Rate constant (K_{ep})	13.607	811673.44	5.352	13.607	*P* < 0.001

Notes: PSA: prostate-specific antigen; PV: prostate volume; ADC: apparent diffusion coefficient.

Table 8. Predictive performance of various MRI parameters for high-risk characteristics in localized prostate cancer

Parameter	Sensitivities	Specificities	AUC	Youden index
PSA level (ng/mL)	0.989	0.545	0.696	0.534
Gleason score	0.849	0.347	0.619	0.196
Tumor Size (cm)	0.591	0.703	0.677	0.294
PV/mL	0.452	0.782	0.620	0.234
T1WI signal intensity	0.559	0.812	0.718	0.371
T2WI signal intensity	0.645	0.772	0.707	0.417
Signal Intensity (50 s/mm^2)	0.667	0.832	0.801	0.499
Signal Intensity (800 s/mm^2)	0.892	0.535	0.783	0.427
ADC (10^{-5} mm^2/s)	0.72	0.703	0.749	0.423
Transfer constant (K^{trans})	0.613	0.822	0.765	0.435
Rate constant (K_{ep})	0.591	0.802	0.745	0.393

Notes: PSA: prostate-specific antigen; PV: prostate volume; ADC: apparent diffusion coefficient.

to construct a joint model for predicting high-risk tumor characteristics in localized prostate cancer. The results revealed an AUC value of 0.826, demonstrating a higher value than each individual parameter. This result indicates that the combined model of diffusion-weighted MRI enhancement parameters holds a strong predictive capability for high-risk tumor characteristics in localized prostate cancer.

Predictive value of joint model integrating standard and diffusion-weighted MRI parameters for high-risk features in localized prostate cancer

As illustrated in **Figure 3**, the combination of standard MRI imaging parameters and enhanced diffusion-weighted MRI parameters to construct a joint model for predicting high-risk tumor characteristics in localized prostate cancer revealed an AUC value of 0.892, higher than their separated prediction values. These results indicate that the combined model of standard imaging and diffusion-weighted MRI parameters holds substantial predictive value for high-risk tumor characteristics in localized prostate cancer.

General patient information in external verification set

In the external validation cohort, the comparison of demographic and health characteristics between the low-risk (n = 80) and high-risk (n = 70) groups revealed no significant differences in age, BMI, smoking history, alcohol consumption, hypertension, diabetes, hyperlipidemia, or family history of prostate cancer (all *P* > 0.05) (**Table 9**). These findings suggest that the two groups were demographically and clinically comparable.

Standard and diffusion-weighted MRI findings in validation set

Both standard and diffusion-weighted MRI parameters showed significant differences between the low risk and high risk groups in the validation set. The low-risk group demonstrated higher T1WI (*t* = 6.374) and T2WI (*t* = 4.707) signal intensities, lower signal intensities at 50

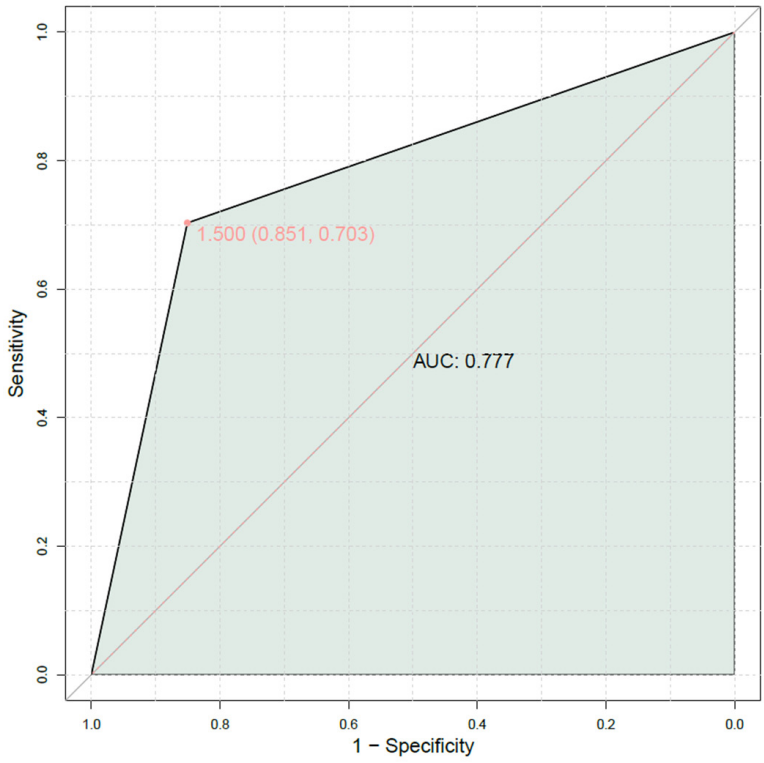

Figure 1. Predictive value of joint model of standard MRI parameters for high-risk characteristics in localized prostate cancer.

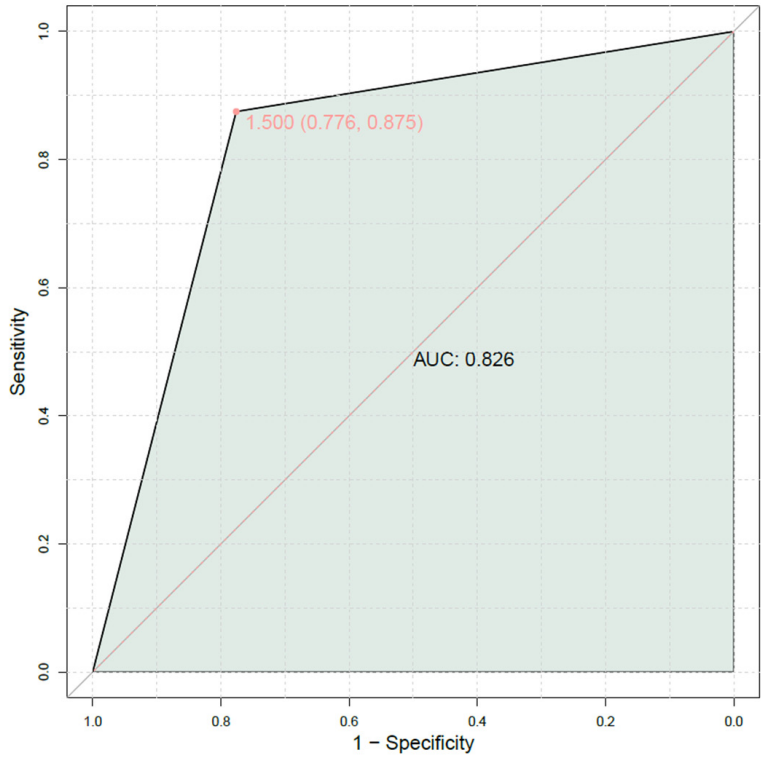

Figure 2. Predictive value of joint model of diffusion-weighted MRI parameters for high-risk characteristics in localized prostate cancer.

s/mm^2 (t = 9.346) and 800 s/mm^2 (t = 6.553), higher ADC values (t = 8.79), and lower transfer constant (K^{trans}) (t = 16.046) and rate constant (K_{ep}) (t = 5.599) compared to the high-risk group (all $P < 0.05$) (**Table 10**). These findings indicate distinct MRI profiles associated with risk categorization in prostate cancer.

Predictive performance of the joint model in validation set

In the validation set, the combined model integrating conventional MRI parameters and diffusion-weighted and contrast-enhanced MRI metrics yielded an AUC value of 0.860, demonstrating excellent predictive performance (**Figure 4**). This validation outcome underscores the efficacy of the joint model in accurately predicting prostate cancer risk, highlighting its potential utility in clinical decision-making.

Discussion

In the comparison of demographic and clinical characteristics between the low and high-risk groups, our study identified significant differences in the PSA level and Gleason score. These observations were consistent with the established clinical understanding that higher PSA levels and Gleason scores were associated with an increased risk of aggressive and advanced prostate cancer [19-21]. While age, BMI, and other clinical characteristics did not display significant differences between the two groups, the PSA level and Gleason score emerged as pivotal indicators of high-risk tumor features. These results underscore the

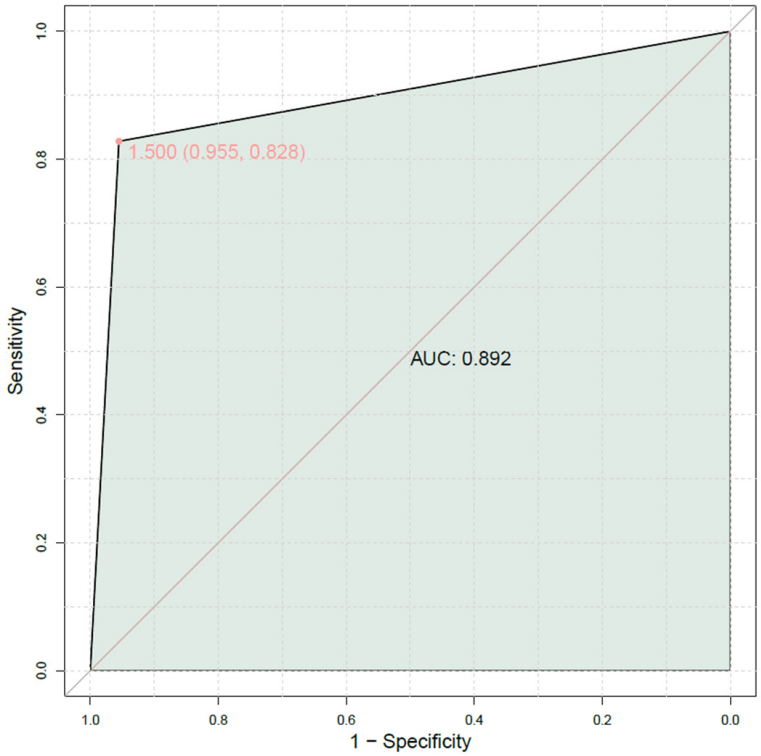

Figure 3. Predictive value of joint model of standard and diffusion-weighted MRI parameters for high-risk characteristics in localized prostate cancer.

importance of these clinical parameters in risk stratification and prognosis assessment for patients with localized prostate cancer.

The findings from the MRI plain scan revealed significant differences in T1WI and T2WI signal intensities between the low-risk and high-risk groups. Lower T1WI and T2WI signal intensities were observed in the high-risk group, suggesting the potential of conventional MRI in delineating high-risk tumor characteristics. This aligns with existing literature that underscores the value of conventional MRI in providing insights into tumor characteristics and guiding clinical decision-making in prostate cancer [22-24]. From a biological perspective, prostate cancer was characterized by heterogeneity in tumor characteristics, encompassing varying degrees of aggressiveness, cellular proliferation, and microstructural alterations. Conventional imaging techniques such as T1-weighted and T2-weighted MRI have been instrumental in capturing macroscopic features of prostate tumors, including size, shape, and anatomical localization [25]. These conventional imaging modalities provide essential anatomical and morphological information, enabling the delineation of tumor boundaries and potential extracapsular extension.

Furthermore, the comparison of diffusion-weighted MRI findings revealed significant differences in signal intensities at different b values, ADC, K^{trans}, and K_{ep} between the low-risk and high-risk groups. Higher signal intensities at b values of 50 s/mm^2 and 800 s/mm^2 and lower ADC values were indicative of high-risk tumor characteristics, reflecting the potential of diffusion-weighted MRI parameters in capturing the aggressiveness and cellular characteristics of localized prostate cancer. These findings were consistent with prior research highlighting the utility of diffusion-weighted MRI in assessing tumor microstructures and cellular density, particularly in the context of prostate cancer [26-28]. By measuring the movement of water molecules within tissues, diffusion-weighted MRI provides insight into tumor cellular density, membrane integrity, and microenvironment [29, 30]. Aggressive tumor features, such as high cellular density, increased cell proliferation, and restricted diffusion, are often associated with high-grade Gleason patterns and extracapsular extension [31]. Consequently, diffusion-weighted MRI parameters, including ADC values and signal intensities at various b-values, can serve as indirect biomarkers of tumor cellularity and aggressiveness.

While this study emphasizes the diagnostic potential of combining conventional imaging and diffusion-weighted MRI enhancement for identifying high-risk tumor characteristics in localized prostate cancer, it is important to address the advantages of this combined imaging approach over other prediction markers. Traditional risk assessment tools, such as PSA levels and Gleason scores, although widely used in clinical practice, have certain limitations in distinguishing between different risk

Table 9. General information and demographic characteristics of patients in the validation set

Characteristic	Low Risk Group (n = 80)	High Risk Group (n = 70)	t/χ^2	*P* Value
Age (years)	59.75 ± 5.77	60.01 ± 5.98	0.304	0.761
BMI (kg/m^2)	25.56 ± 2.52	26.04 ± 2.64	1.300	0.195
Smoking history	16 (20.00%)	18 (25.71%)	0.206	0.650
Alcohol consumption history	8 (10.00%)	12 (17.14%)	0.817	0.366
Hypertension [n (%)]	30 (37.50%)	28 (40.00%)	0.000	1.000
Diabetes [n (%)]	21 (26.25%)	18 (25.71%)	0.005	0.944
Hyperlipidemia [n (%)]	26 (32.50%)	22 (31.43%)	0.029	0.865
Family history of prostate cancer (Yes/No)	24 (30.00%)	28 (40.00%)	0.696	0.404

Note: BMI: body mass index.

Table 10. Comparison of various MRI parameters between the low- and high-risk groups in the validation set

Parameter		Low risk (n = 80)	High risk (n = 70)	t	*P* Value
T1WI signal intensity		287.24 ± 27.48	258.57 ± 34.44	6.374	$P < 0.001$
T2WI signal intensity		301.57 ± 17.96	285.04 ± 29.14	4.707	$P < 0.001$
Signal Intensity	50 s/mm^2	85.65 ± 6.83	95.68 ± 8.02	9.346	$P < 0.001$
	800 s/mm^2	100.42 ± 10.78	109.57 ± 8.62	6.553	$P < 0.001$
ADC (10^{-5} mm^2/s)		106.75 ± 10.26	94.51 ± 9.13	8.79	$P < 0.001$
Transfer constant (K^{trans})		0.27 ± 0.06	0.39 ± 0.05	16.046	$P < 0.001$
Rate constant (K_{ep})		0.66 ± 0.09	0.73 ± 0.06	5.599	$P < 0.001$

Note: ADC: apparent diffusion coefficient.

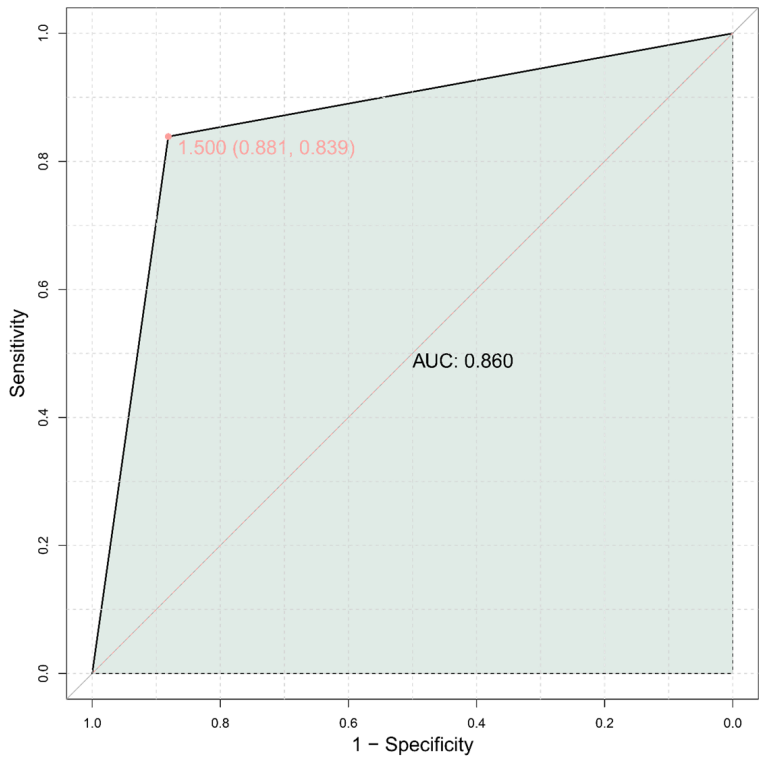

Figure 4. Predictive value of joint models in validation set.

levels of prostate cancer. PSA levels can be influenced by multiple factors, such as prostatitis or benign prostatic hyperplasia, leading to false-positive results. Similarly, Gleason scores rely on histopathological assessments, which may be influenced by sampling errors and lack comprehensiveness. In contrast, the combined use of conventional imaging and diffusion-weighted MRI provides more intuitive and quantitative information, better reflecting the biological behavior and microenvironmental characteristics of the tumor. Diffusion-weighted imaging, by measuring the diffusion of water molecules within tissue, reveals changes in tumor cell density and microstructure, offering a unique perspective on tumor aggressiveness and heterogeneity.

Additionally, dynamic contrast-enhanced MRI parameters such as the transfer constant (K^{trans}) and rate constant (K_{ep}) reflect tumor vascular permeability and perfusion, further enhancing diagnostic accuracy. Therefore, this integrated imaging approach not only improves the precision of risk stratification but also supports the development of personalized treatment strategies.

The correlation analysis further strengthened the association between standard imaging and diffusion-weighted MRI parameters with high-risk features of localized prostate cancer. Positive correlations were observed for PSA level and Gleason score, while negative correlations were noted for T1WI and T2WI signal intensities with high-risk features. Additionally, diffusion parameters such as signal intensities at different b values, ADC, K^{trans}, and K_{ep} displayed significant correlations with high-risk tumor characteristics. These correlations emphasize the potential of these imaging parameters as valuable biomarkers for risk assessment and prognostication in localized prostate cancer.

The logistic regression analysis provided insights into the independent risk factors for high-risk tumor characteristics in localized prostate cancer. Both standard imaging parameters and diffusion-weighted MRI parameters emerged as independent predictors, with notable coefficients and odds ratios. Notably, K^{trans} and K_{ep} exhibited substantial coefficients, signifying their potential as robust predictors of high-risk tumor characteristics. These results emphasize the utility of MRI parameters in risk prediction and risk stratification, laying the foundation for their integration into clinical practice for improved patient management in localized prostate cancer.

The predictive value of standard imaging and diffusion-weighted MRI parameters were further supported by the ROC analysis, which yielded promising results. T2WI signal intensity exhibited high specificity and sensitivity, with a substantial AUC, highlighting its potential as a reliable biomarker for identifying high-risk tumor characteristics. Additionally, signal intensity at 800 s/mm^2 and ADC displayed meaningful AUC values, further underlining their diagnostic potential. These results emphasize the clinical relevance of these imaging parameters in risk assessment and treatment planning for localized prostate cancer. In addition, a validation set of patients was used to further confirm the predictive performance of this model. The results showed excellent predictive value of the model, confirming the utility of integrating both standard imaging and diffusion-weighted MRI parameters for improving diagnostic accuracy.

Moreover, the construction of joint prediction models utilizing standard imaging and diffusion-weighted MRI parameters highlighted their combined predictive value for high-risk tumor characteristics in localized prostate cancer. The high AUC values obtained for these joint models underscore their potential clinical utility as comprehensive risk assessment tools. The combination of conventional imaging and diffusion-weighted MRI enhances the complementary information derived from both modalities. While conventional imaging provides macroscopic anatomical details, diffusion-weighted MRI offers microstructural insights, thereby facilitating a comprehensive assessment of tumor characteristics. This combined approach harnesses the strengths of each modality, allowing for a more comprehensive and nuanced evaluation of tumor aggressiveness and risk stratification. The ability to capture both macroscopic and microscopic features of prostate tumors contributes to the robust diagnostic potential of the combined imaging approach. Moreover, technological advancements in MRI hardware, software, and imaging protocols have further optimized the diagnostic capabilities of conventional and diffusion-weighted MRI. High-field MRI systems, advanced coil designs, and refined imaging sequences have enhanced spatial resolution, signal-to-noise ratio, and image quality, enabling the precise visualization of subtle anatomical and microstructural changes in the prostate gland. These technical developments have empowered radiologists and clinicians to discern high-risk tumor characteristics with higher accuracy and confidence, thereby elevating the clinical utility of MRI in localized prostate cancer management.

While the findings of this study present significant contributions to the field of imaging-based risk stratification in localized prostate cancer, several limitations should be acknowledged. The retrospective nature of the study introduces inherent biases, and the findings should be

validated through prospective studies with larger sample sizes. Additionally, the generalizability of the results may be influenced by the single-center design, highlighting the need for multi-center studies to corroborate the observed associations. Furthermore, the study focused on a specific cohort of patients, and the applicability of the findings to diverse patient populations needs to be examined. Future research should also explore the integration of advanced imaging modalities and multi-parametric approaches to further enhance risk assessment and treatment decision-making in localized prostate cancer. Research [32] has shown that the methylation status of LGALS3 cfDNA in semen can effectively distinguish early prostate cancer (PCa) from benign prostatic hyperplasia (BPH), and its performance as a prostate cancer biomarker far exceeds traditional prostate-specific antigen (PSA) detection. This discovery may provide a new method for early diagnosis of prostate cancer.

Conclusion

In conclusion, our study highlights the diagnostic potential of combining conventional and diffusion-weighted MRI parameters in identifying high-risk tumor characteristics in patients with localized prostate cancer. The observed associations between standard imaging and diffusion-weighted MRI parameters with high-risk features underscore their value as non-invasive biomarkers for risk assessment and prognostication. These findings hold implications for precision treatment of localized prostate cancer, offering insights into the potential integration of imaging-based risk assessment tools into clinical practice for tailored treatment strategies and improved patient outcomes. Nonetheless, further research endeavors are warranted to validate these findings and explore the broader clinical applicability of imaging-based risk stratification in localized prostate cancer.

Disclosure of conflict of interest

None.

Address correspondence to: Peijun Liu, Department of Radiology, The Affiliated Nanhua Hospital, Hengyang Medical School, University of South China, No. 336 Dongfeng South Road, Zhuhui District, Hengyang 421002, Hunan, China. E-mail: juns4368@163.com

References

[1] Carlsson SV and Vickers AJ. Screening for prostate cancer. Med Clin North Am 2020; 104: 1051-1062.

[2] Wasim S, Lee SY and Kim J. Complexities of prostate cancer. Int J Mol Sci 2022; 23: 14257.

[3] Schaeffer EM, Srinivas S, Adra N, An Y, Barocas D, Bitting R, Bryce A, Chapin B, Cheng HH, D'Amico AV, Desai N, Dorff T, Eastham JA, Farrington TA, Gao X, Gupta S, Guzzo T, Ippolito JE, Kuettel MR, Lang JM, Lotan T, McKay RR, Morgan T, Netto G, Pow-Sang JM, Reiter R, Roach M, Robin T, Rosenfeld S, Shabsigh A, Spratt D, Teply BA, Tward J, Valicenti R, Wong JK, Shead DA, Snedeker J and Freedman-Cass DA. Prostate cancer, version 4.2023, NCCN clinical practice guidelines in oncology. J Natl Compr Canc Netw 2023; 21: 1067-1096.

[4] Williams IS, McVey A, Perera S, O'Brien JS, Kostos L, Chen K, Siva S, Azad AA, Murphy DG, Kasivisvanathan V, Lawrentschuk N and Frydenberg M. Modern paradigms for prostate cancer detection and management. Med J Aust 2022; 217: 424-433.

[5] Achard V, Putora PM, Omlin A, Zilli T and Fischer S. Metastatic prostate cancer: treatment options. Oncology 2022; 100: 48-59.

[6] Sekhoacha M, Riet K, Motloung P, Gumenku L, Adegoke A and Mashele S. Prostate cancer review: genetics, diagnosis, treatment options, and alternative approaches. Molecules 2022; 27: 5730.

[7] Albertsen PC. PSA testing, cancer treatment, and prostate cancer mortality reduction: what is the mechanism? Urol Oncol 2023; 41: 78-81.

[8] Kachuri L, Hoffmann TJ, Jiang Y, Berndt SI, Shelley JP, Schaffer KR, Machiela MJ, Freedman ND, Huang WY, Li SA, Easterlin R, Goodman PJ, Till C, Thompson I, Lilja H, Van Den Eeden SK, Chanock SJ, Haiman CA, Conti DV, Klein RJ, Mosley JD, Graff RE and Witte JS. Genetically adjusted PSA levels for prostate cancer screening. Nat Med 2023; 29: 1412-1423.

[9] Maestroni U, Cavalieri DM, Campobasso D, Guarino G and Ziglioli F. PSA-IgM and iXip in the diagnosis and management of prostate cancer: clinical relevance and future potential. A review. Acta Biomed 2022; 92: e2021344.

[10] Penney KL, Tyekucheva S, Rosenthal J, El Fandy H, Carelli R, Borgstein S, Zadra G, Fanelli GN, Stefanizzi L, Giunchi F, Pomerantz M, Peisch S, Coulson H, Lis R, Kibel AS, Fiorentino M, Umeton R and Loda M. Metabolomics of prostate cancer gleason score in tumor tissue

and serum. Mol Cancer Res 2021; 19: 475-484.
[11] Swanson GP, Trevathan S, Hammonds KAP, Speights VO and Hermans MR. Gleason score evolution and the effect on prostate cancer outcomes. Am J Clin Pathol 2021; 155: 711-717.
[12] Wang X, Zhang Y, Ji Z, Yang P and Tian Y. Old men with prostate cancer have higher risk of Gleason score upgrading and pathological upstaging after initial diagnosis: a systematic review and meta-analysis. World J Surg Oncol 2021; 19: 18.
[13] Siegel DA, O'Neil ME, Richards TB, Dowling NF and Weir HK. Prostate cancer incidence and survival, by stage and race/ethnicity - United States, 2001-2017. MMWR Morb Mortal Wkly Rep 2020; 69: 1473-1480.
[14] Wu RC, Lebastchi AH, Hadaschik BA, Emberton M, Moore C, Laguna P, Fütterer JJ and George AK. Role of MRI for the detection of prostate cancer. World J Urol 2021; 39: 637-649.
[15] Jendoubi S, Wagner M, Montagne S, Ezziane M, Mespoulet J, Comperat E, Estellat C, Baptiste A and Renard-Penna R. MRI for prostate cancer: can computed high b-value DWI replace native acquisitions? Eur Radiol 2019; 29: 5197-5204.
[16] Eastham JA, Boorjian SA and Kirkby E. Clinically localized prostate cancer: AUA/ASTRO guideline. J Urol 2022; 208: 505-507.
[17] Freedman S and Wickramasekera IE 2nd. Review of the international hypnosis literature. Am J Clin Hypn 2020; 62: 159-165.
[18] Iczkowski KA, van Leenders GJLH and van der Kwast TH. The 2019 International Society of Urological Pathology (ISUP) consensus conference on grading of prostatic carcinoma. Am J Surg Pathol 2021; 45: 1007.
[19] Maffei D, Giganti F and Moore CM. Seminar: revisiting the value of PSA-based prostate cancer screening Essay No 5: should men undergo MRI before prostate biopsy? (Pro). Urol Oncol 2023; 41: 88-91.
[20] Msheik A, Mohanna M, Mhanna A, Kanj A, Moussa M and Mohanna A. Predictive value of PSA density in the diagnosis of prostate cancer in lebanese men. Arch Ital Urol Androl 2022; 94: 18-24.
[21] Lysenko I, Mori K, Mostafaei H, Enikeev DV, Karakiewicz PI, Briganti A, Quhal F, Janisch F and Shariat SF. Prognostic value of gleason score at positive surgical margin in prostate cancer: a systematic review and meta-analysis. Clin Genitourin Cancer 2020; 18: e517-e522.
[22] Fernandes MC, Yildirim O, Woo S, Vargas HA and Hricak H. The role of MRI in prostate cancer: current and future directions. MAGMA 2022; 35: 503-521.
[23] Murgić J, Gregov M, Mrčela I, Budanec M, Krengli M, Fröbe A and Franco P. MRI-guided radiotherapy for prostate cancer: a new paradigm. Acta Clin Croat 2022; 61 Suppl 3: 65-70.
[24] Stempel CV, Dickinson L and Pendsé D. MRI in the management of prostate cancer. Semin Ultrasound CT MR 2020; 41: 366-372.
[25] O'Shea A and Harisinghani M. PI-RADS: multiparametric MRI in prostate cancer. MAGMA 2022; 35: 523-532.
[26] Maier SE, Wallström J, Langkilde F, Johansson J, Kuczera S, Hugosson J and Hellström M. Prostate cancer diffusion-weighted magnetic resonance imaging: does the choice of diffusion-weighting level matter? J Magn Reson Imaging 2022; 55: 842-853.
[27] Tamada T, Ueda Y, Ueno Y, Kojima Y, Kido A and Yamamoto A. Diffusion-weighted imaging in prostate cancer. MAGMA 2022; 35: 533-547.
[28] Wu D, Jiang K, Li H, Zhang Z, Ba R, Zhang Y, Hsu YC, Sun Y and Zhang YD. Time-dependent diffusion MRI for quantitative microstructural mapping of prostate cancer. Radiology 2022; 303: 578-587.
[29] Abdelmaksoud IR, Shalaby A, Mahmoud A, Elmogy M, Aboelfetouh A, Abou El-Ghar M, El-Melegy M, Alghamdi NS and El-Baz A. Precise identification of prostate cancer from DWI using transfer learning. Sensors (Basel) 2021; 21: 3664.
[30] Hectors SJ, Said D, Gnerre J, Tewari A and Taouli B. Luminal water imaging: comparison with diffusion-weighted imaging (DWI) and PI-RADS for characterization of prostate cancer aggressiveness. J Magn Reson Imaging 2020; 52: 271-279.
[31] Adorno Febles VR, Hao Y, Ahsan A, Wu J, Qian Y, Zhong H, Loeb S, Makarov DV, Lepor H, Wysock J, Taneja SS, Huang WC, Becker DJ, Balar AV, Melamed J, Deng FM, Ren Q, Kufe D, Wong KK, Adeegbe DO, Deng J and Wise DR. Single-cell analysis of localized prostate cancer patients links high Gleason score with an immunosuppressive profile. Prostate 2023; 83: 840-849.
[32] Abramovic I, Pezelj I, Dumbovic L, Skara Abramovic L, Vodopic T, Bulimbasic S, Stimac G, Bulic-Jakus F, Kulis T, Katusic Bojanac A, Tomas D, Ulamec M and Sincic N. LGALS3 cfDNA methylation in seminal fluid as a novel prostate cancer biomarker outperforming PSA. Prostate 2024; 84: 1128-1137.